

Identification of the Mechanical Subsystem of the NEES-UCSD Shake Table by a Least-Squares Approach

O. Ozcelik¹; J. E. Luco²; and J. P. Conte³

Abstract: A least-squares method is used to determine the fundamental parameters of a simple mathematical model for the mechanical subsystem of the NEES-UCSD large high performance outdoor shaking table. The parameters identified include the effective horizontal mass, the effective horizontal stiffness, and the coefficient of the classical Coulomb friction and viscous damping elements representing the various dissipative forces in the system. The values obtained for these parameters are validated by comparisons with previous results based on an alternative identification method applicable only to periodic tests and by comparisons with experimental data obtained during earthquake simulation tests and harmonic steady-state tests. The proposed identification approach works well for periodic sinusoidal and triangular tests, earthquake simulation tests, and white noise tests with table root mean square above 10% of gravity.

DOI: 10.1061/(ASCE)0733-9399(2008)134:1(23)

CE Database subject headings: Shake table tests; Least squares method; Earthquakes; Simulation.

Introduction

Objectives of the Study

The new UCSD-NEES large high performance outdoor shaking table (LHPOST) located at the Englekirk Structural Engineering Center at Camp Elliot Field Station, a site 15 km away from the main UCSD campus, is a unique facility that enables next generation seismic experiments to be conducted on very large structural and soil-foundation-structure-interaction systems. Large tests of a 21 m tall wind turbine, and a tall seven story, reinforced concrete shear wall building model (Fig. 1) have been conducted on the table. Optimization of the shake table performance during the tests, as well as the optimization of the experiments themselves, including sensor location and safety precautions, requires the use of a detailed and reliable mathematical model of the complete facility. In general, a complete model of a shake table system needs to include the mechanical, hydraulic, and electronic subsystems. Typically, the steel platen, vertical and lateral bearings, hold-down struts, and actuators are included in the mechanical subsystem; pumps, accumulator bank, line accumulators, servovalves, and surge tank are part of the hydraulic subsystem; and finally, controller, signal conditioners, sensors, and built-in analog filters are included in the electronic subsystem.

In a previous paper (Ozcelik et al. 2007), the authors devel-

oped a simplified analytical model for the mechanical subsystem of the UCSD-NEES shaking table, identified the parameters of the model using the data collected during the extensive shake down tests of the table, and validated the model by detailed comparisons with experimental data. The model and parameter identification approach used in the previous study were based on analysis of the hysteresis loops relating the feedback total actuator force to the feedback displacement, velocity, and acceleration of the platen recorded during periodic tests (both triangular and harmonic). The procedure took advantage of the periodicity of the motion of the table during sinusoidal or triangular tests, to isolate the inertial, elastic, and dissipative forces and their respective dependence on acceleration, displacement, and velocity. The approach is restricted to periodic tests, but does not assume a priori a linear model. Since the table motion for most future pretests will consist of scaled down seismic motions or random white noise acceleration signals, it is necessary to develop and test identification methods that do not depend on the periodicity of the excitation.

The first objective of this study is to test the applicability of a parameter identification approach based on the standard least-squares method for shake table tests with very different excitations including periodic tests, white noise tests, and seismic tests. Of primary interest is the robustness of the parameter estimates across different types of tests. A second objective is to compare the results of the least-squares identification approach with those obtained by consideration of the hysteresis loops for periodic tests. A third objective of the study is to further validate the model and identify parameters by detailed comparisons with experimental data from different types of tests. Finally, the steady-state frequency response of the shake table mechanical subsystem to commanded harmonic displacement of the shake table is examined. This analysis provides an additional verification of the nonlinear damping model used in the study, and illustrates the response of the table in the vicinity of the characteristic frequency of the mechanical subsystem. It is envisioned that the analytical model of the mechanical subsystem obtained in this and the pre-

¹Dept. of Structural Engineering, Univ. of California, San Diego, 9500 Gilman Dr., La Jolla, CA 92093-0085.

²Dept. of Structural Engineering, Univ. of California, San Diego, 9500 Gilman Dr., La Jolla, CA 92093-0085.

³Dept. of Structural Engineering, Univ. of California, San Diego, 9500 Gilman Dr., La Jolla, CA 92093-0085.

Note. Associate Editor: Lambros S. Katfygiotis. Discussion open until June 1, 2008. Separate discussions must be submitted for individual papers. To extend the closing date by one month, a written request must be filed with the ASCE Managing Editor. The manuscript for this paper was submitted for review and possible publication on February 9, 2007; approved on May 30, 2007. This paper is part of the *Journal of Engineering Mechanics*, Vol. 134, No. 1, January 1, 2008. ©ASCE, ISSN 0733-9399/2008/1-23-34/\$25.00.



Fig. 1. Seven-story full-scale R/C building slice, 19.2 m high

vious paper (Ozcelik et al. 2007) will be used in future studies to model the entire shake table system including all subsystems mentioned previously.

It is expected that the present study will add to the growing literature on the modeling of shake table systems (Hwang et al. 1987; Rinawi and Clough 1991; Clark 1992; Conte and Trombetti 2000; Williams et al. 2001; Shortreed et al. 2001; Crewe and Severn 2001; Trombetti and Conte 2002; Twitchell and Symans 2003; Thoen and Laplace 2004).

Overview of the UCSD-NEES Shake Table

The LHPOST consists of a moving steel platen (7.6 m wide by 12.2 m long); a reinforced concrete reaction block; two servo-controlled dynamic actuators with a force capacity in tension/compression of 2.6 and 4.2 MN, respectively; a platen sliding

system (six pressure balanced vertical bearings with a force capacity of 9.4 MN each and a stroke of ± 0.013 m); an overturning moment restraint system (a prestressing system consisting of two nitrogen-filled hold-down struts with a stroke of 2 m and a hold-down force capacity of 3.1 MN each); a yaw restraint system (two pairs of slaved pressure balanced bearings along the length of the platen); a real-time multivariable controller; and a hydraulic power supply system. The technical specifications of the LHPOST include a stroke of ± 0.75 m, a peak horizontal velocity of 1.8 m/s, a peak horizontal acceleration of 4.2 g for bare table conditions and 1.0 g for a rigid payload of 3.92 MN, a horizontal force capacity of 6.8 MN, an overturning moment capacity of 50 MN m, and a vertical payload capacity of 20 MN. The frequency bandwidth is 0–20 Hz. Other detailed specifications of the NEES-UCSD LHPOST can be found elsewhere (Van Den Einde et al. 2004).

Experimental Data

The experimental data used to model and identify the fundamental characteristics of the UCSD-NEES shake table were recorded during shake-down tests, which were performed in the period June–September, 2004 to verify that the performance of the shake table complies with the design specifications.

The tests designed for system characterization and identification purposes include periodic, earthquake, and white noise tests. For the periodic tests, sinusoidal (S) and triangular (T) waveforms were used with amplitude and frequency characteristics carefully selected so as to span the entire operational frequency range of the system. For the earthquake tests, full and scaled versions of historic earthquake records with different characteristics were used. Finally, several white noise tests with different root mean square table accelerations were performed on the system. All of these tests were incorporated in the identification process to make sure that the identified fundamental characteristics of the system do not change across test types and test characteristics. The details of the tests performed on the system are summarized in Tables 1 and 2.

Triangular and sinusoidal tests were performed with zero, 1,042.4 kN (6.9 MPa nitrogen pressure), and 2,084.8 kN (13.8 MPa nitrogen pressure) forces in each of the two hold-down struts in order to determine the effective horizontal stiffness produced by the hold-down struts, and also to investigate the effect of vertical forces on the dissipative (friction, damping) forces. All

Table 1. Characteristics of the Triangular and Sinusoidal Tests Performed on the System

Tests	Displacement (cm)	Velocity (cm/s)	Frequency (Hz)	Tests	Displacement (cm)	Velocity (cm/s)	Acceleration (g)	Frequency (Hz)
T1	5.00	1.00	0.05	S1	4.00	1.00	0.0003	0.04
T2	7.50	1.50	0.05	S2	4.00	1.51	0.0006	0.06
T3	12.50	2.50	0.05	S3	4.00	2.51	0.0016	0.10
T4	50.00	10.00	0.05	S4	4.00	10.05	0.0257	0.40
T5	25.00	10.00	0.10	S5	4.00	25.12	0.1608	1.00
T6	62.50	25.00	0.10	S6	10.00	25.12	0.0643	0.40
T7	37.50	25.00	0.167	S7	10.00	50.24	0.2573	0.80
T8	75.00	50.00	0.167	S8	10.00	75.36	0.5789	1.20
T9	46.88	75.00	0.40	S9	20.00	75.36	0.2895	0.60
T10	62.50	100.00	0.40	S10	20.00	100.48	0.5146	0.80
T11	75.00	150.00	0.50	S11	20.00	150.72	1.1578	1.20
T12	67.50	180.00	0.667	S12	20.00	179.61	1.6442	1.43

Table 2. Characteristics of Earthquake and White Noise Tests Performed on the System

Tests	PGA (g)	rms amplitude (g)	Scaling (%)
El Centro—1	0.07	—	20
El Centro—2	0.37	—	100
El Centro—3	1.11	—	300
Northridge	1.84	—	100
WN3%g	0.12	0.03	100
WN5%g	0.22	0.05	100
WN7%g	0.32	0.07	100
WN10%g	0.45	0.10	100
WN13%g	0.49	0.13	100

triangular waves were rounded at their peak displacement values (at the change of velocity) with a phase of duration equal to one-tenth of the wave period and constant acceleration not exceeding 2 g. All earthquake and white noise tests were performed with a force of 2,084.8 kN (13.8 MPa nitrogen pressure) in each of the two hold-down struts. All triangular, sinusoidal, earthquake, and white noise tests were conducted several times in order to check for repeatability of the results.

The total actuator force recorded during the last two sine and triangular tests, namely S11, S12, T11, and T12, which had a maximum velocity near the velocity capacity of the table, were distorted to such an extent that they could not be used for the purpose of parameter identification. For this reason, these four tests were not considered in all facets of this study.

Sensors and Data Acquisition System

Data were acquired by the built-in sensors and data acquisition (DAQ) system used for controlling the shaking table. The sampling frequency of the DAQ system is set at the default rate of 1,024 Hz. This DAQ system also has low-pass antialiasing filtering capabilities. The displacement of the platen relative to the reaction block was measured by two digital displacement transducers (Temposonics linear transducers) located on the east and west actuators. The platen acceleration response was measured by two Setra-Model 141A accelerometers with a range of ± 8 g and a flat frequency response from DC to 300 Hz. It should be noted here that the signal conditioners used for the accelerometers include a built-in analog low-pass filter with cutoff frequency set at 100 Hz, implying that acceleration records have frequency content only up to 100 Hz. Pressure in the various actuator chambers was measured by four Precise Sensors-Model 782 pressure transducers (located in the tension and compression chambers of each actuator) with a pressure range from 0 to 68.9 MPa and a (sensor/DAQ) resolution of 689.5 Pa. These pressure transducers are located near the end caps of each actuator. Measured pressures are converted to actuator forces by multiplying them with the corresponding actuator piston areas and combining the contributions from both chambers. At this point, it is important to mention that pressure recordings were high-pass filtered to remove their static pressure components, but were not low-pass filtered. The velocity of the platen is the only response quantity measured indirectly. To obtain a wideband estimate of velocity, the differentiated displacement sensor signal is combined with the integrated acceleration sensor signal via a crossover filter. This filter ensures that the velocity estimate of the platen consists primarily of differentiated displacement at low-to-medium frequencies for which the dis-

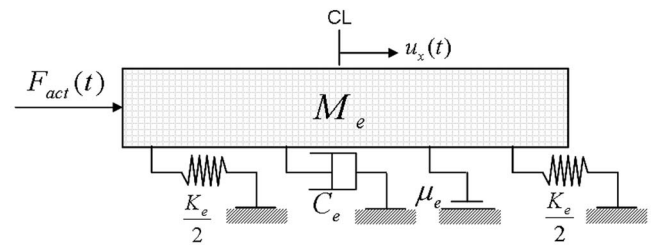


Fig. 2. Conceptual mechanical model of the table with model parameters M_e , K_e , C_e , and F_{μ_e} to be identified through periodic, earthquake, and white noise tests

placement sensor is more accurate, and integrated acceleration at medium-to-high frequencies for which the acceleration sensor is more accurate (Thoen 2004).

The MTS 469D Seismic Controller Recorder software was used to record the digitized data; this software is an integral part of the MTS 469D Digital Controller. The sampling rate of this software can be set at a different rate than the one used by the controller (1,024 Hz). The sampling rate of the recorder was set at 512 Hz during the tests. Again, to prevent aliasing, the anti aliasing digital filter built in the recorder was enabled during the tests. The sampling rate used on the recorder was sufficiently high for all the tests performed on the system.

To interpret the results presented in the following sections, two important general observations about the recorded data need to be pointed out here. In all the tests performed, two harmonic signals at 10.66 Hz and 246 Hz were observed repeatedly, mainly in the total force and table acceleration records. The signal at 10.66 Hz corresponds to the oil column frequency of the system. The effective table mass of the system and the oil column within the actuators give rise to a mass-spring system with a natural frequency referred to as the oil column frequency (Thoen and Laplace 2004; Conte and Trombetti 2000; Kusner et al. 1992). This oil column resonance frequency tends to be excited when there is a sudden change in the motion of the platen such as a direction reversal. The most likely source of the second harmonic signal at 246 Hz is the resonance between the pilot stage and the third stage of the servovalves. Due to low-pass filtering of the acceleration records at 100 Hz, this 246 Hz harmonic signal can be observed only slightly in the acceleration records, but it is clearly observed in the actuator force records that are only subjected to high-pass filtering. The discrepancy between the filtering of the actuator force and platen acceleration data does not allow to simulate the high frequency harmonic components of the total actuator force by use of the recorded table motion.

Model and Parameter Estimation by Least-Squares Approach

Conceptual Model

A detailed analysis of the dynamics of the platen and hold-down struts (Ozcelik et al. 2007) indicates that several nonlinear terms affecting the inertial and elastic forces are small and can be neglected. Under these conditions, a simplified mathematical model of the shake table system with a relatively small number of unknown parameters can be formulated. This model is represented in Fig. 2, where $F_{act}(t)$ =total effective actuator force applied on the pistons of the two horizontal actuators; M_e =effective mass

of the platen (including the mass of the moving parts of the horizontal actuators and a portion of the mass of the hold-down struts); K_e =total effective horizontal stiffness provided by the two hold down struts; C_e =effective viscous damping coefficient; F_{μ_e} =effective Coulomb friction force due to various sources; and $u_x(t)$ =total horizontal displacement of the platen along the longitudinal direction.

According to this simplified model, the equation of motion of the shake table can be written as

$$M_e \ddot{u}_x(t) + K_e u_x(t) + [C_e |\dot{u}_x(t)|^\alpha + F_{\mu_e}] \text{sign}[\dot{u}_x(t)] = F_{\text{act}}(t) \quad (1)$$

where the exponent α is a constant. The model parameters to be identified (M_e , K_e , C_e , F_{μ_e} , α) are all effective in nature, as different sources are lumped into the same type of resisting force (e.g., various physical sources of energy dissipation contribute to the viscous damping coefficient C_e).

Basic Least-Squares Formulation

The parameters (M_e , K_e , C_e , F_{μ_e}) of the mathematical model given in Eq. (1) are identified by use of the linear least-squares method for a given value of α . The objective function to be minimized is given by

$$\bar{\epsilon}^2 = \frac{\sum_{i=1}^N \lambda_i \int_0^{T_i} [F_{\text{act}}(t) - M_e \ddot{u}_x - K_e u_x - (C_e |\dot{u}_x|^\alpha + F_{\mu_e}) \text{sign}(\dot{u}_x)]^2 dt}{\sum_{j=1}^N \lambda_j \int_0^{T_j} F_{\text{act}}^2(t) dt} \quad (2)$$

where $\bar{\epsilon}$ =normalized error to be minimized for a given value of α ; N =number of tests considered; T_i =duration of the i th test; and λ_i =weight assigned to the i th test. Eq. (2) can be rewritten in the following alternative form:

$$\bar{\epsilon}^2 = 1 + \mathbf{y}^T \mathbf{a} \mathbf{y} - \mathbf{b}^T \mathbf{y} - \mathbf{y}^T \mathbf{b} \quad (3)$$

where \mathbf{y} , \mathbf{a} , and \mathbf{b} are defined as

$$\mathbf{y}^T = (M_e, K_e, C_e, F_{\mu_e}) \quad (4)$$

$$\mathbf{a} = \sum_{i=1}^N \bar{\lambda}_i \int_0^{T_i} \mathbf{R} \mathbf{R}^T dt \quad (5)$$

$$\mathbf{b} = \sum_{i=1}^N \bar{\lambda}_i \int_0^{T_i} \mathbf{R} F_{\text{act}}(t) dt \quad (6)$$

in which

$$\mathbf{R}^T = \{\ddot{u}_x(t), u_x(t), |\dot{u}_x(t)|^\alpha \text{sign}[\dot{u}_x(t)], \text{sign}[\dot{u}_x(t)]\} \quad (7)$$

The normalized weights $\bar{\lambda}_i$ appearing in Eqs. (5) and (6) are defined as

$$\bar{\lambda}_i = \frac{\lambda_i}{\sum_{j=1}^N \lambda_j \int_0^{T_j} F_{\text{act}}^2(t) dt} \quad (8)$$

Vectors \mathbf{y} and \mathbf{R} =parameter vector and measured response vector, respectively. It should be noted that the components of the response vector \mathbf{R} as well as the actuator force $F_{\text{act}}(t)$ are known from the recorded test data.

The model parameters \mathbf{y}_0 that minimize the error measure $\bar{\epsilon}^2$ satisfy the normality conditions

$$\frac{\partial \bar{\epsilon}^2}{\partial \mathbf{y}} = \mathbf{0} \quad (9)$$

that after consideration of Eq. (3) leads to

$$\mathbf{a} \mathbf{y}_0 = \mathbf{b} \quad (10)$$

After finding the optimum parameters \mathbf{y}_0 by solving Eq. (10), the minimum squared error can be obtained as

$$\bar{\epsilon}_0^2 = 1 - \mathbf{b}^T \mathbf{y}_0 \quad (11)$$

Since the tests performed on the system involve widely different amplitudes (Table 1 and Table 2), it is necessary to consider the use of weighting factors λ_i . For this purpose, we define ϵ_i as the normalized weighted error in the i th test for the optimum values of the parameters as

$$\epsilon_i = \frac{\int_0^{T_i} [F_{\text{act}}(t) - M_e \ddot{u}_x - K_e u_x - (C_e |\dot{u}_x|^\alpha + F_{\mu_e}) \text{sign}(\dot{u}_x)] F_{\text{act}}(t) dt}{\int_0^{T_i} F_{\text{act}}^2(t) dt} \quad (12)$$

By using Eq. (12), the minimum squared error $\bar{\epsilon}_0^2$ can be written as

$$\bar{\epsilon}_0^2 = \sum_{i=1}^N \left\{ \bar{\lambda}_i \left[\int_0^{T_i} F_{\text{act}}^2(t) dt \right] \epsilon_i \right\} \quad (13)$$

One possible choice for the weights λ_i is given by

$$\lambda_i = 1 / \int_0^{T_i} F_{\text{act}}^2(t) dt \quad (14)$$

In this case, the minimum squared error reduces to

$$\bar{\epsilon}_0^2 = \frac{1}{N} \sum_{i=1}^N \epsilon_i \quad (15)$$

indicating that the choice of λ_i given in Eq. (14) has the advantage of assigning equal relative importance to all tests, regardless of their force amplitudes.

A second possible choice is to select $\lambda_i=1$ ($i=1, \dots, N$). In this case, the minimum squared error takes the form

$$\bar{\epsilon}_0^2 = \sum_{i=1}^N \left[\int_0^{T_i} F_{\text{act}}^2(t) dt / \sum_{j=1}^N \int_0^{T_j} F_{\text{act}}^2(t) dt \right] \epsilon_i \quad (16)$$

indicating that the tests performed at lower force amplitudes are given less relative importance than those performed at larger force amplitudes. Many other choices are possible for λ_i and some are considered in the sequel.

Estimation of Parameter α

The proposed linear least-squares approach to determine the model parameters (M_e , K_e , C_e , F_{μ_e}) presumes that the parameter α controlling the viscous dissipative force model ($C_e |\dot{x}|^\alpha$) is known. In an attempt to determine the optimum value of α , the minimum least-squares error $\bar{\epsilon}_0$ was computed for a set of values of α in the range from 0.0 to 1.0. In this process, all the

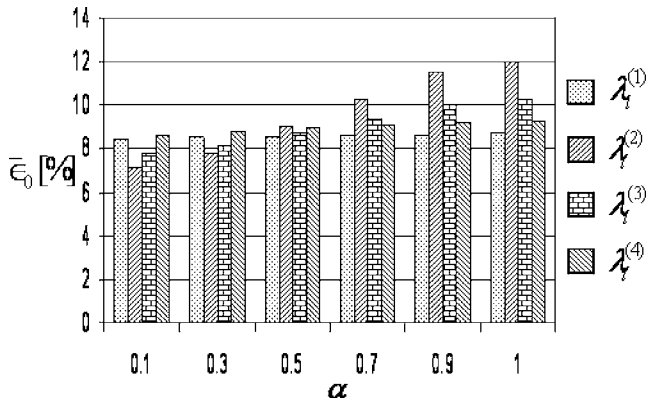


Fig. 3. Minimum least-squares error $\bar{\epsilon}_0$ as a function of parameter α and for different types of weights λ_i ($i=1 \dots 12$)

triangular tests for a nitrogen pressure of 13.8 MPa in the hold-down struts were considered with four choices for the weights λ_i , namely, $\lambda_i^{(1)}=1$, $\lambda_i^{(2)}=1/\int_0^T (\dot{u}_x)^2 dt$, $\lambda_i^{(3)}=1/[\int_0^T (\dot{u}_x)^2 dt]^{1/2}$, and $\lambda_i^{(4)}=1/\int_0^T F_{act}^2(t) dt$ were used.

The results obtained for $\bar{\epsilon}_0$ as a function of α and the types of weights λ_i are presented in Fig. 3, which shows that $\bar{\epsilon}_0$ is relatively independent of the types of weights λ_i and of the value of parameter α . These results indicate that the overall minimum least-squares error combining several tests may not be the best criterion to determine the optimum value of the parameter α . Instead, the stability of the parameters C_e and F_{μ_e} identified from individual tests at different amplitudes is used to determine the optimum value of parameter α . Thus, the least-squares identification procedure was applied separately to the data from each of the sinusoidal Tests S1 through S10 of increasing peak velocity for several values of parameter α . The resulting estimates of F_{μ_e} and C_e for $\alpha=1$ and $\alpha=1/2$ are presented in Fig. 4. In the case of a linear viscous force model ($\alpha=1$), the estimate of the Coulomb friction force F_{μ_e} is relatively constant from test to test [Fig. 4(a)], but the viscous coefficient C_e decreases with test order and velocity [Fig. 4(c)]. This result indicates that the dissipative forces during sinusoidal tests cannot be represented by a simple combination of Coulomb friction and linear viscous damping. The results for a nonlinear viscous force ($\alpha=1/2$) show a more constant estimate for C_e [Fig. 4(d)], but the estimated friction force F_{μ_e} changes somewhat from test to test in this case [Fig. 4(b)]. Attempts with other values of α do not lead to results significantly more uniform than those obtained for $\alpha=1/2$. Thus, the value $\alpha=1/2$ was adopted in this study.

Figs. 4(e and f) show the estimated total dissipative force at the maximum achieved velocity for each test plotted versus the peak velocity. The total dissipative force is calculated as

$$F_d = (C_e |\dot{u}_x|^\alpha + F_{\mu_e}) \text{sign}(\dot{u}_x) \quad (17)$$

where F_{μ_e} and C_e =parameter values estimated by the least-squares approach for each particular test. Comparison of the results in Figs. 4(e and f) indicate that two significantly different models ($\alpha=0.5$ and $\alpha=1.0$) lead to essentially the same total dissipative force. Thus, it appears that individual test data may not be sufficient to discriminate between the different combinations of α , F_{μ_e} , and C_e (i.e., eliminate compensation effects).

Equivalent Linear Viscous Damper

To understand the tradeoffs between the Coulomb friction force $F_{\mu_e} \text{sign}(\dot{u}_x)$ and the viscous damping force $C_e |\dot{u}_x|^\alpha \text{sign}(\dot{u}_x)$, it is convenient to introduce an equivalent linear viscous damper characterized by the damping coefficient \tilde{C}_e . This constant \tilde{C}_e is defined such that the energy dissipated by the equivalent linear viscous damper over a cycle of periodic response of duration T is equal to that dissipated by the complete model in Eq. (17). The resulting expression for \tilde{C}_e is given by

$$\tilde{C}_e = \gamma_1 F_{\mu_e} / \nu + \gamma_2 C_e / \nu^{1-\alpha} \quad (18)$$

where ν denotes the peak velocity, and

$$\gamma_1 = \nu \int_0^T |\dot{u}_x| dt / \int_0^T \dot{u}_x^2 dt \quad (19)$$

$$\gamma_2 = \nu^{1-\alpha} \int_0^T |\dot{u}_x|^{1+\alpha} dt / \int_0^T \dot{u}_x^2 dt \quad (20)$$

In the particular case of a periodic triangular test with velocity ν and period T , it can be shown that $\gamma_1=\gamma_2=1$ and $\tilde{C}_e=F_{\mu_e}/\nu + C_e/\nu^{1-\alpha}$. In the case of a sinusoidal test with velocity $\dot{u}_x(t)=\nu \sin(2\pi t/T)$ characterized by the peak velocity ν and period T , the factors γ_1 and γ_2 become

$$\gamma_1 = \left(\frac{4}{\pi} \right) \quad (21)$$

$$\gamma_2 = \frac{2^\alpha}{\pi} \left(\frac{\alpha}{1+\alpha} \right) \frac{\Gamma^2(\alpha/2)}{\Gamma(\alpha)} \quad (22)$$

where $\Gamma(\cdot)$ denotes the gamma function. In particular, for the special case $\alpha=1/2$, then $\gamma_1=1.273$, $\gamma_2=1.113$, and $\tilde{C}_e = 1.273 F_{\mu_e} / \nu + 1.113 C_e / \sqrt{\nu}$.

Eq. (18) indicates that for a given value of the peak velocity ν , different combinations of F_{μ_e} and C_e can lead to the same equivalent linear viscous damping coefficient and thus to the same total energy dissipation. Hence, to properly identify the Coulomb and viscous dissipative forces, it is necessary to consider simultaneously several tests with very different velocities. The last term in Eq. (18) and the results in Fig. 4(c) for the estimated linear viscous damping coefficient ($\alpha=1$) suggest that an effective viscous damper with a fractional power law is a more suitable representation of the data.

In what follows, the data from different sets of tests will be pooled together, and the parameter α will be set to 0.5 on the basis of the relative stability of the estimates of F_{μ_e} and C_e obtained from different tests. The resulting estimates of M_e , K_e , and of the total dissipative force are relatively independent of the assumed value for the parameter α .

Parameter Estimation

The parameter identification was conducted separately for nine sets of pooled data. Three of the sets consist of the combination of ten sinusoidal tests for hold-down pressures of 0, 6.9, and 13.8 MPa, respectively. A second group of three sets involve the combination of ten triangular tests also for hold-down nitrogen pressures of 0, 6.9, and 13.8 MPa, respectively. The seventh set corresponds to the three scaled El Centro seismic tests at the

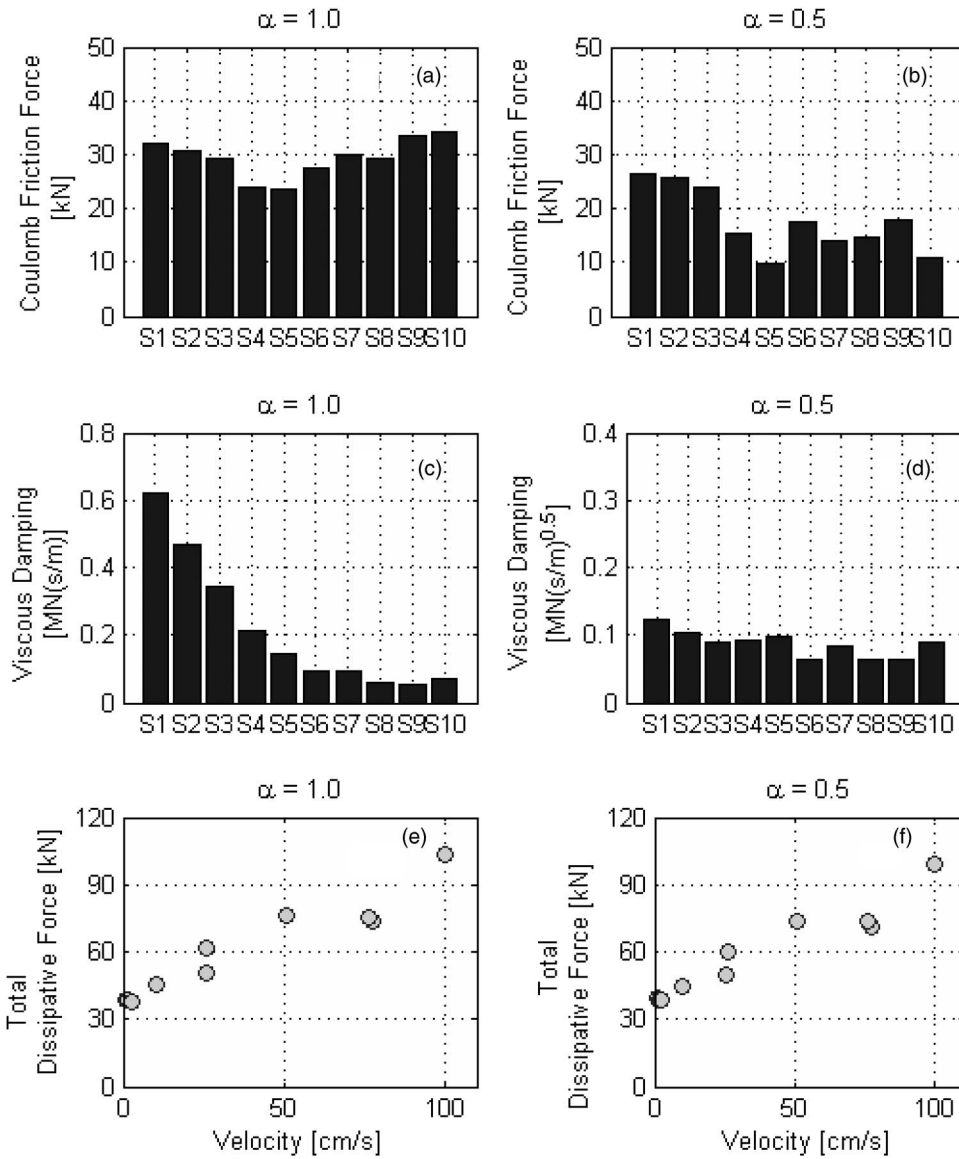


Fig. 4. (a), (b): Coulomb friction forces; (c), (d): viscous damping coefficient; and (e), (f): total dissipative force estimated from each of ten different sine tests for $\alpha=1.0$ and $\alpha=0.5$

operating hold-down nitrogen pressure of 13.8 MPa. The eighth set consists of data from three white noise tests with rms amplitudes of 0.03, 0.05, and 0.07 g, respectively, conducted at the operating hold-down nitrogen pressure. Finally, the ninth set is defined by two white noise tests with rms amplitudes of 0.10 and 0.13 g, respectively, conducted at the operating hold-down nitrogen pressure.

Effective Mass Estimation

The results of the least-squares identification for the effective mass M_e are presented in Table 3 for two choices of the weights corresponding to $\lambda_i = \lambda_i^{(1)}$ and $\lambda_i = \lambda_i^{(2)}$. With one exception, the estimated effective masses obtained from different test types, different nitrogen pressure conditions in the hold-down struts, and different weights are in good agreement. It appears that M_e increases slightly with the nitrogen pressure in the hold-down struts, thus suggesting some correlation with the effective stiffness K_e . The average of the estimates of M_e for the periodic tests

Table 3. Estimates of the Effective Mass of the System for Different Test Types and Different Levels of Nitrogen Pressure in the Hold-Down Struts ($\alpha=0.5$)

Test type—nitrogen pressure	M_e (tons)	
	$\lambda_i = \lambda_i^{(1)}$ $i=1, \dots, 12$	$\lambda_i = \lambda_i^{(2)}$ $i=1, \dots, 12$
Sine—0.0 MPa	134.7	114.1
Triangular—0.0 MPa	138.4	139.0
Sine—6.9 MPa	143.2	143.5
Triangular—6.9 MPa	144.3	144.4
Sine—13.8 MPa	143.9	144.5
Triangular—13.8 MPa	143.9	143.8
El Centro tests—13.8 MPa	146.2	145.7
WN (0.03, 0.05, 0.07 g rms)—13.8 MPa	143.6	143.5
WN (0.10, 0.13 g rms)—13.8 MPa	144.0	144.0

Table 4. Estimates of the Effective Horizontal Stiffness of the Hold-Down Struts for Different Test Types and Different Levels of Nitrogen Pressure in the Hold-Down Struts ($\alpha=0.5$)

Test type—nitrogen pressure	K_e [MN/m]	
	$\lambda_i=\lambda_i^{(1)}$ $i=1, \dots, 12$	$\lambda_i=\lambda_i^{(2)}$ $i=1, \dots, 12$
	Sine—6.9 MPa	0.611
Triangular—6.9 MPa	0.644	0.645
Sine—13.8 MPa	1.246	1.281
Triangular—13.8 MPa	1.261	1.262
El Centro tests—13.8 MPa	1.221	1.255
WN (0.03, 0.05, 0.07 g rms)—13.8 MPa	1.916	2.132
WN (0.10, 0.13 g rms)—13.8 MPa	1.392	1.417

at the hold-down nitrogen operating pressure of 13.8 MPa is 144 tons. The estimate of M_e from the white noise tests at 0.10 and 0.13 g rms acceleration is also 144 tons, matching the average result for the triangular and sine tests. The average estimates of the effective mass from the white noise tests with smaller amplitudes (0.03–0.05–0.07 g rms acceleration) is 143.6 tons, which is also close to the average estimate from the periodic tests. The estimates of M_e from higher frequency earthquake tests are on the average of 1.4% larger than those obtained from lower frequency triangular and sine tests.

The one deficient estimate of the effective system mass occurs for the sinusoidal tests at zero hold-down nitrogen pressure and for the weights $\lambda_i=\lambda_i^{(2)}$. The problem is associated with the low amplitudes, velocities, and accelerations achieved during Tests S1 through S4. When these four tests are removed from the pool, the estimate of the effective mass increases from 114.1 to 146.9 tons. In addition, when all S1 through S10 tests are used but the viscous damping coefficient is constrained (as described later), then the estimate of the effective mass is 146.1 tons.

Effective Horizontal Stiffness Estimation

The results obtained for the effective horizontal stiffness K_e are reported in Table 4. It should be noted here that for tests corresponding to zero nitrogen pressure in the hold-down struts, there is no horizontal stiffness acting on the system.

The estimates of the effective stiffness K_e obtained from the periodic tests increase linearly with the nitrogen pressure in the

hold-down struts from an average value of 0.635 MN/m for a pressure of 6.9 MPa to an average value of 1.263 MN/m for a pressure of 13.8 MPa. The triangular tests involve larger forces in the hold-down struts and smaller inertia forces than the sinusoidal tests and appear to yield more stable estimates of K_e .

The average estimate of K_e obtained from the El Centro tests is 1.238 MN/m, which is 2% lower than the corresponding average estimate obtained from the periodic tests. The results in Tables 3 and 4 indicate that for the earthquake tests there is some compensation effects between the estimates of M_e and K_e , with M_e being 1.3% larger and K_e 2% lower than the corresponding estimates from the periodic tests. The average estimate of K_e from the 0.10 and 0.13 g rms acceleration white noise tests is 1.405 MN/m, which is 11.2% larger than the corresponding average estimate from the periodic tests. The estimates of K_e based on the low-amplitude (0.03, 0.05, and 0.07 g rms acceleration) white noise tests are significantly higher than the other estimates and appear to be in error. The low amplitude white noise tests involve extremely small displacements, but significant accelerations. Under these conditions, the elastic forces are much smaller than the inertia forces, and the stiffness cannot be determined accurately.

From the above results, it can be concluded that the effective horizontal stiffness of the system is approximately 1.263 MN/m in the nominal case corresponding to a nitrogen pressure of 13.8 MPa in the hold-down struts. For a nitrogen pressure of 6.9 MPa, the effective stiffness is reduced to 0.63 MN/m.

Estimation of Dissipative Force

The estimates of the dissipative force parameters F_{μ_e} and C_e obtained from the nine pooled sets of data for $\alpha=0.5$ and weighting factors ($\lambda_i=\lambda_i^{(1)}$ and $\lambda_i=\lambda_i^{(2)}$) are reported in Table 5 in the columns labeled “unconstrained.” The results indicate that both F_{μ_e} and C_e increase with the hold-down nitrogen pressure. The average values of F_{μ_e} over the two weighting factors and the two types of tests (triangular and sinusoidal), are 16.7, 25.9, and 29.5 kN for the three hold-down nitrogen pressures (0.0, 6.9, and 13.8 MPa). The corresponding average values of C_e are 18.4, 34.5, and 46.0 kN(s/m)^{0.5}. Although the unconstrained estimates of F_{μ_e} are fairly stable for a given hold-down nitrogen pressure, the corresponding unconstrained estimates of C_e vary significantly with weighting factor and test type.

A second set of estimates for F_{μ_e} was obtained by repeating the least-squares based estimation process with C_e constrained to

Table 5. Estimates of Coulomb Friction Force and Viscous Damping Coefficients Obtained by Least-Squares Approach with Pooled Datasets ($\alpha=0.5$)

Tests types—nitrogen pressure	Unconstrained				Constrained			
	F_{μ_e} (kN)		C_e [kN (s/m) ^{1/2}]		F_{μ_e} (kN)		C_e [kN (s/m) ^{1/2}]	
	$\lambda^{(1)}$	$\lambda^{(2)}$	$\lambda^{(1)}$	$\lambda^{(2)}$	$\lambda^{(1)}$	$\lambda^{(2)}$	$\lambda^{(1)}$	$\lambda^{(2)}$
Sine—0.0 MPa	17.4	16.6	21.4	17.6	12.4	5.7	45.9	45.9
Triangular—0.0 MPa	17.1	15.8	13.1	21.5	8.7	5.9	45.9	45.9
Sine—6.9 MPa	26.1	26.8	41.1	36.1	23.8	19.8	45.9	45.9
Triangular—6.9 MPa	24.8	26.0	31.2	29.4	20.7	24.2	45.9	45.9
Sine—13.8 MPa	30.1	30.6	49.4	48.4	27.5	23.9	45.9	45.9
Triangular—13.8 MPa	27.9	29.2	42.3	43.8	25.9	28.6	45.9	45.9
El Centro tests—13.8 MPa	25.6	28.0	51.3	62.1	26.4	30.2	45.9	45.9
WN (0.03, 0.05, 0.07 g rms)—13.8 MPa	14.14	14.6	140.03	149.8	25.8	26.3	45.9	45.9
WN (0.10, 0.13 g rms)—13.8 MPa	9.19	9.4	120.21	123.1	24.3	24.4	45.9	45.9

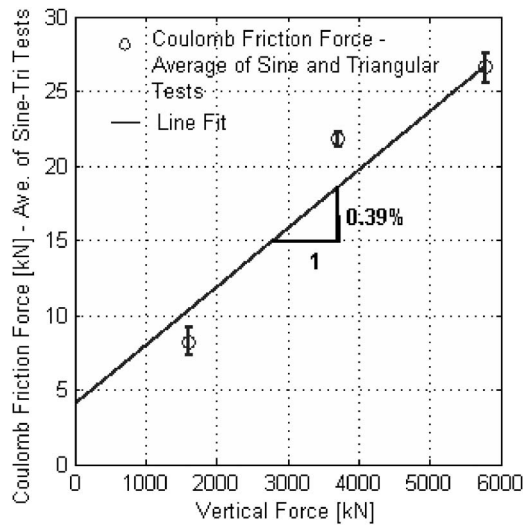


Fig. 5. Average Coulomb friction forces ($\lambda^{(1)}$ and $\lambda^{(2)}$) as a function of total vertical force on vertical bearings (dispersion bounds for sine and triangular tests)

be equal to $46.0 \text{ [kN(s/m)}^{0.5}]$ corresponding to the average estimate of C_e over the sinusoidal and triangular tests for a hold-down nitrogen pressure of 13.8 MPa. The resulting constrained estimates of F_{μ_e} are also given in Table 5. The constrained estimates of F_{μ_e} are more stable across test type and weighting factor. The average constrained value of F_{μ_e} over the sinusoidal and triangular tests and the two weighting factors are 8.2, 22.1, and 26.5 kN for the hold-down nitrogen pressures of 0, 6.9, and 13.8 MPa, respectively. The constrained estimates of the friction force F_{μ_e} from the scaled El Centro tests and from the two sets of white noise tests are 28.3, 26.1, and 24.4 kN, respectively, which are close to the average estimate of 26.5 from the periodic tests. The deviations from the average of the periodic tests are as high as 8%, but these differences amount to less than 2.1 kN, which is well within the margin of error in estimating the dissipative forces from the measured data.

Both the constrained and unconstrained estimates of F_{μ_e} suggest that the friction forces depend on the hold-down nitrogen pressure and, consequently, are mostly associated with friction on the vertical bearings of the platen. The unconstrained estimates of the effective viscous damping coefficient C_e also depend on the hold-down nitrogen pressure, suggesting that the dissipative viscous forces are also related to the vertical bearings. The constrained estimate of C_e is selected to be independent of the hold-down nitrogen pressure and would be consistent with viscous forces in the lateral bearings of the platen and in the actuators, instead of the vertical bearings. Both sets of estimates of F_{μ_e} and C_e lead to essentially the same total dissipative forces (within the margin of error) and, consequently, it is not possible to discriminate between these two possibilities. The constrained estimates will be used in the sequel.

The results given in Table 5 indicate that the constrained estimate of F_{μ_e} based on the scaled El Centro tests is within 7% of the average value of F_{μ_e} based on sinusoidal and triangular tests. The corresponding difference for white noise tests is less than 8%. Thus, the constrained least-squares approach can identify the total friction force from a variety of tests.

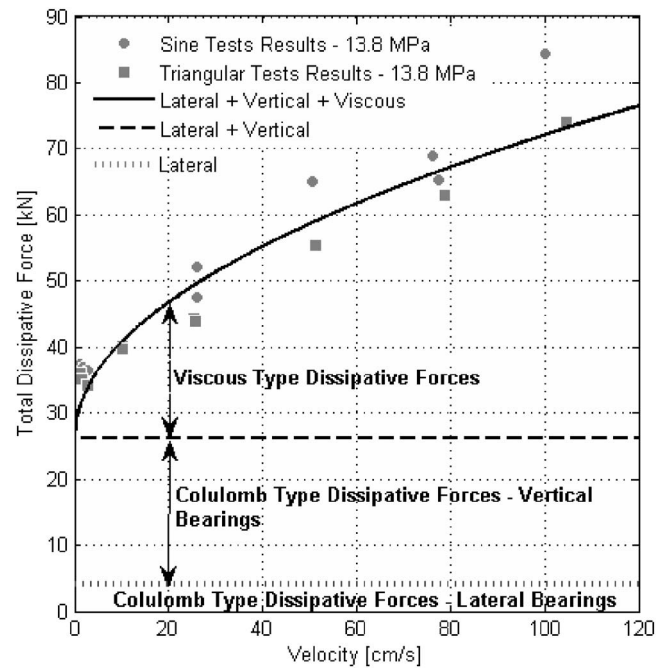


Fig. 6. Decomposition of the total dissipative force into its three major components

Decomposition of the Total Friction Force

The two major sources of Coulomb-type friction in the system are the vertical and lateral bearings. The inferred values for the total friction force F_{μ_e} obtained from tests performed under different hold-down nitrogen pressures can be used to quantify these two sources of friction. The average of the estimates of F_{μ_e} obtained from sinusoidal and triangular tests for different levels of nitrogen pressure in the hold-down struts are shown in Fig. 5 versus the total corresponding vertical force acting on the vertical bearings. The total vertical force was obtained experimentally from readings of the pressures on the vertical bearings for the different hold-down pressures. The forces correspond to 1.613, 3.698, and 5.783 MN for hold-down nitrogen pressures of 0.0, 6.9, and 13.8 MPa, respectively. A least-squares fit to the three points thus obtained leads to a line with a slope of 0.39% and an intercept of 4.1 kN. It appears then that the total friction force F_{μ_e} can be expressed as $F_{\mu_e} = F_{\mu_{e,lat}} + \mu_e F_z$, where F_z = total vertical force acting on the vertical bearings; $F_{\mu_{e,lat}} = 4.1 \text{ kN}$ = friction force exerted by the lateral bearings; and $\mu_e = 0.39\%$ = Coulomb friction coefficient in the vertical bearings.

A decomposition of the dissipative forces into friction components on the horizontal and vertical bearings and viscous forces is presented in Fig. 6, based on tests performed under the nominal hold-down nitrogen pressure of 13.8 MPa. Similar results were found from triangular tests performed under the same hold-down nitrogen pressure.

The results in Fig. 6 indicate that for a table velocity of 75 cm/s, for example, 6% of the total dissipative force is due to Coulomb friction on the lateral bearings, 34% to Coulomb friction on the vertical bearings, and 60% to viscous damping forces.

Fig. 6 also shows a comparison between the total dissipative force obtained by use of the overall inferred model represented by Eq. (1) (curve in Fig. 6) and the corresponding forces obtained through (constrained) least-squares parameter estimation for

Table 6. Comparison of Model Parameters Estimated from Two Different Methods Based on Data from Periodic Tests (Sinusoidal and Triangular) Performed under Nominal Hold-Down Nitrogen Pressure of 13.8 MPa

Model parameters	Least squares	Hysteresis loops approach
M_e (tons)	144	144
K_e (MN/m)	1.263	1.266
C_e [kN(s/m) ^{0.5}]	46.0	44.6
μ_e (%)	0.39	0.45
$F_{\mu, \text{lat}}$ (kN)	4.1	0.0
F_{μ_e} (kN)	26.7	26.0

individual sinusoidal and triangular tests (symbols in Fig. 6). It is observed that the inferred model slightly underestimates the total dissipative force for sinusoidal tests, but overestimates the total dissipative force for triangular tests.

Comparison of Parameters Identified by Periodic, White Noise, and Earthquake Simulation Tests

Before comparing the parameter identification results obtained by applying the least-squares method to different types of tests including periodic, white noise, and earthquake tests, a comparison of the results obtained from two different identification methods based on periodic sinusoidal and triangular test data is presented. The values of the parameters identified in the present paper by the (constrained) least-squares approach are compared in Table 6 with those obtained previously (Ozcelik et al. 2007) by analysis of the observed hysteresis loops. The estimates of the effective mass M_e and effective stiffness K_e obtained using the two identification methods are in excellent agreement. The details of the parameters related to the dissipative forces are slightly different, but the values of the viscous damping coefficient C_e are within 3%. In addition, the total static Coulomb friction forces F_{μ_e} obtained by the two methods differ by 2.7% corresponding to 0.7 kN, which is well below the margin of error. The results obtained by the least-squares approach led to slightly larger dissipative forces (2.8% at a velocity of 1 m/s), but the difference amounts to about 2.0 kN for a velocity of 1 m/s.

Next, we examine the stability of the results of parameter identification by the least-squares method when applied to different types of tests including periodic, white noise, and earthquake tests. A summary of the results obtained is presented in Table 7. Comparison of the results indicates that for the scaled earthquake tests, the estimated mass is slightly larger (1.4%), the estimated stiffness slightly smaller (2.0%), and the (constrained) friction

force slightly larger (6.8%) than for the periodic tests. The estimate of the effective mass based on the white noise tests is accurate, but the effective stiffness is overestimated.

Table 7 includes two sets of estimates for the viscous damping coefficient C_e and the Coulomb friction force. In the first set, the values of C_e were left unconstrained while in the second set, the constants C_e were constrained to 45.9 kN (s/m)^{0.5}. It is apparent that the constrained parameter estimation results for the Coulomb friction are similar across the various types of tests, but the unconstrained estimates of the viscous damping coefficient and Coulomb friction force obtained from the white noise tests are in error.

In conclusion, the least-squares approach appears to be equally capable of identifying the key system parameters from scaled earthquake tests and periodic sinusoidal and triangular tests. For white noise tests, the approach leads to the correct effective mass, but the obtained values for the other parameters are questionable.

Experimental Validation of the Proposed Model of the NEES-UCSD Shake Table Mechanical System

Comparison between Analytical and Experimental Total Actuator Force

The results of the least-squares parameter identification obtained here are very similar to those obtained previously by analysis of the observed hysteresis loops. Those results had been validated by detailed comparisons of simulated and recorded actuator forces for Test T4, 100% Northridge earthquake simulation test, and a white noise test with a 10% g root mean square amplitude (Ozcelik et al. 2007). As additional validation, the total actuator force recorded during the 300% El Centro earthquake test will be compared with the simulated actuator force obtained from Eq. (1) using the recorded actual table displacement, velocity, and acceleration as inputs and $\alpha=0.5$.

Fig. 7 shows a 2 s segment of the recorded and simulated total actuator force time histories for the El Centro earthquake record scaled to PGA=1.11 g. It is observed that the analytical prediction based on the estimated model parameters given above is in excellent agreement with the recorded total actuator force. An alternative way of comparing test results with simulations is presented in Fig. 8 that shows plots of recorded and simulated total actuator forces versus recorded platen velocities for the 300% El Centro earthquake test. For sake of clarity, only 1 s segment of the test is shown. Again, the agreement between analytical and experimental results is excellent.

Table 7. Comparison of Model Parameters Identified Based on Periodic, Earthquake, and White Noise Tests (Hold-Down Nitrogen Pressure of 13.8 MPa)

Model parameters	Periodic tests	El Centro tests	White noise tests (10–13% g rms)	White noise tests (3–5–7% g rms)
M_e (tons)	144.0	146.0	144.0	143.6
K_e (MN/m)	1.263	1.238	1.405	2.024
C_e [kN(s/m) ^{0.5}] ^a	45.9	45.9	45.9	45.9
Coulomb friction force (kN) ^a	26.5	28.3	24.4	26.1
C_e [kN(s/m) ^{0.5}] ^b	45.9	57.6	121.7	144.9
Coulomb friction force (kN) ^b	27.7	26.8	9.3	14.4

^a C_e constrained.

^b C_e unconstrained.

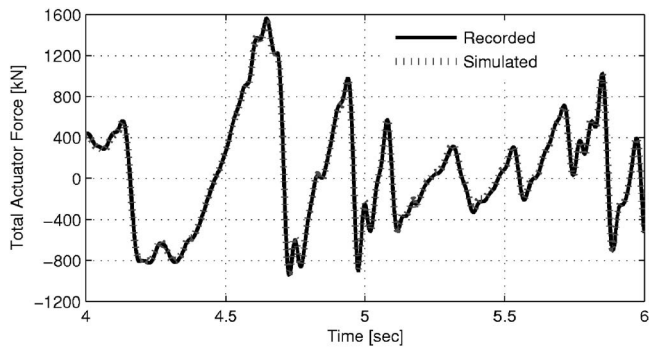


Fig. 7. Comparison of recorded and simulated total actuator forces for the 300% El Centro earthquake test (13.8 MPa nitrogen pressure in the hold-down struts)

Comparison between Analytical and Experimental Steady-State Frequency Response

The mechanical system described by Eq. (1) has an undamped natural frequency given by $\omega_e = \sqrt{K_e/M_e}$ corresponding to a frequency of 0.471 Hz (period of 2.12 s). One way of testing the energy dissipation model included in Eq. (1) is to consider the steady-state response of the system to harmonic excitation with frequencies in the vicinity of the system's natural frequency ω_e . In the vicinity of ω_e , the inertial and elastic forces approximately cancel each other, and the actuator force is approximately equal to the damping force.

With the above objective in mind, the equation of motion of the system [Eq. (1)] was integrated numerically for a sinusoidal actuator force $F_{act}(t) = F_0 \sin(2\pi ft)$, and the peak amplitude u_{max} of the steady-state displacement was obtained for different values of the excitation frequency f and the force amplitude F_0 . Theoretical dynamic amplification factors $R_d = u_{max}/(F_0/K_e)$ for different values of F_0 in the range from 49 to 250 kN were calculated and are shown versus frequency f (in Hz) in Fig. 9 in the form of several frequency response curves. Shown also in Fig. 9 are the values of the experimental ratios $u_{max}/(F_{max}/K_e)$ obtained

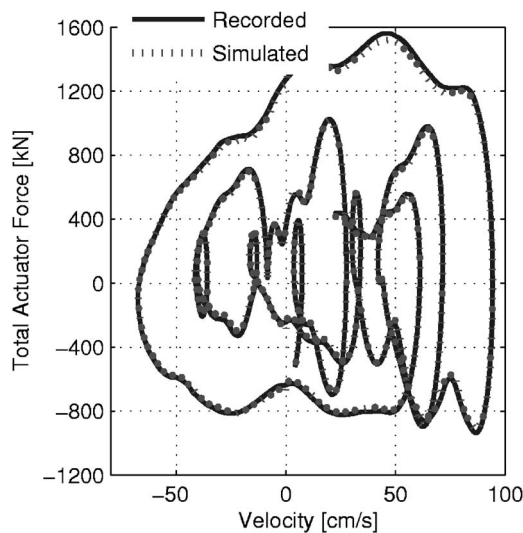


Fig. 8. Recorded and simulated total actuator force versus recorded table velocity plots for 300% El Centro earthquake test (13.8 MPa pressure in the hold-down struts)

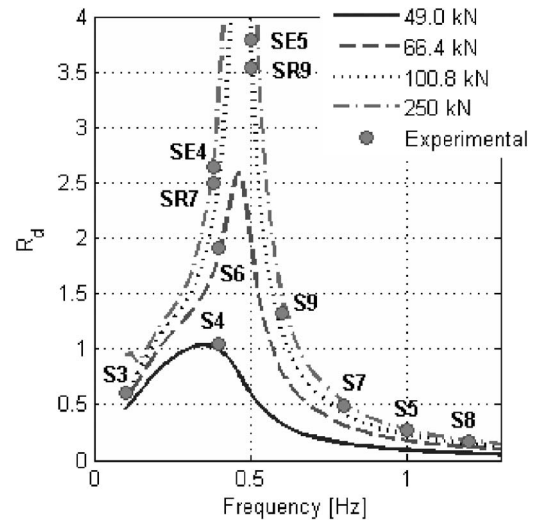


Fig. 9. Dynamic amplification curves for the nonlinear model in Eq. (1) of the NEES-UCSD shake table mechanical system

for several sinusoidal tests plotted versus the frequency of the test. Since the system is nonlinear, these two ratios are not strictly comparable. In the experimental ratio, u_{max} = maximum value of the feedback table displacement (which may not be exactly sinusoidal) and F_{max} = peak value of the recorded total actuator force, which also may not be exactly sinusoidal. In the theoretical dynamic amplification factor R_d , the actuator force is sinusoidal, but the calculated displacement response is not exactly sinusoidal. In spite of these differences, the theoretical dynamic amplification factors (curves in Fig. 9) and the experimental ratios (black dots in Fig. 9) follow the same trends. The experimental ratios for Tests S3, SR7, and SE4, all with frequencies below the frequency of the system, fall on the left branches of the dynamic amplification curves. The measured peak actuator forces during these tests were 83, 262, and 384 kN, respectively, and the corresponding experimental ratios fall close to the dynamic amplification curves shown for 100.8 and 250 kN. The experimental ratios for Tests SE5, SR9, S9, S7, and S5, which have peak actuator forces in the range from 133 to 242 kN, fall between the descending branches of the dynamic amplification curves for 100 and 250 kN. The experimental ratio for Test S6, which has a peak actuator force of 66.4 kN falls on the dynamic amplification curve for 66.4 kN. Finally, the experimental ratio for Test S4 with a peak actuator force of 49 kN falls very close to the amplification curve for 49 kN. The comparisons between analytical and experimental results in Fig. 9 give further indication that the inferred model of the NEES-UCSD shake table mechanical system is consistent with the data.

A better understanding of the dynamic response of the shake table can be reached by obtaining estimates of the equivalent linear viscous damping ratio ξ_e for different velocities of the table. This equivalent damping ratio can be obtained from

$$\xi_e = \frac{\tilde{C}_e}{2M_e\omega_e} \quad (23)$$

where \tilde{C}_e = equivalent viscous damping coefficient given by Eq. (18). Substitution from Eq. (18) into Eq. (23) leads to

Table 8. Equivalent Linear Viscous Damping Ratio ξ_e for Different Platen Velocities and Characteristics of Peak Amplification Points

v (cm/s)	ξ_e (%)	f_m (Hz)	A_m —	u_{\max} (cm)	F_0 (kN)
20.00	33.20	0.416	1.60	7.65	60.5
25.12	27.72	0.433	1.88	9.23	62.2
50.24	16.32	0.458	3.11	17.46	71.1
75.36	12.15	0.464	4.15	25.85	78.9
100.5	9.91	0.466	5.07	34.32	85.7
125.00	8.52	0.468	5.89	42.51	91.2
150.72	7.50	0.468	6.69	51.26	97.0
180.00	6.67	0.469	7.52	61.08	102.8

$$\xi_e = \frac{\gamma_1}{2} \left(\frac{F_{\mu_e}}{K_e} \right) \frac{\omega_e}{v} + \frac{\gamma_2}{2} \left(\frac{C_e \omega_e}{K_e} \right) \frac{1}{v^{1-\alpha}} \quad (24)$$

where v = peak table velocity in m/s. After substitution of the inferred values of the model parameters, Eq. (24) reduces to

$$\xi_e = (3.97/v + 5.97/\sqrt{v})/100 \quad (25)$$

Numerical values for the equivalent linear viscous damping ratio ξ_e for different platen velocities are given in Table 8.

The approximate equivalent linear viscous damping ratio ξ_e can be used to estimate the frequency f_m at which the amplification ratio reaches its peak value A_m . The standard relations for the equivalent linear system are

$$f_m = f_e \sqrt{1 - 2\xi_e^2} \quad A_m = 1/(2\xi_e \sqrt{1 - \xi_e^2}) \quad (26)$$

where $f_e = 2\pi/\omega_e$. The amplitudes of the platen displacement and the actuator force at the peak amplification point (f_m, A_m) are given by $u_{\max} = v/(2\pi f_m)$, and $F_0 = K_e u_{\max}/A_m$, respectively. The values of f_m, A_m, u_{\max} , and F_0 are also given in Table 8. The points (f_m, A_m) as a function of u_{\max}, v , or F_0 describe the approximate locus of the peak amplification points in Fig. 9 and can be used to define future sinusoidal tests of the shake table that would help to further validate the dissipative force model described herein.

Conclusions

In this paper, the parameters characterizing a mathematical model of the mechanical subsystem of the NEES-UCSD large shake table are estimated from test data by use of a least-squares approach. The parameters identified include the effective mass, effective horizontal stiffness induced by the nitrogen-filled hold-down struts, the Coulomb friction forces on the vertical and lateral bearings, and the effective viscous damping coefficients.

In the case of periodic sinusoidal and triangular tests, the parameter estimates obtained in the present paper by the least-squares approach are in close agreement with those obtained previously (Ozcelik et al. 2007) by analysis of the observed hysteresis loops. The effective mass M_e and effective horizontal stiffness K_e obtained by two methods are essentially the same. The viscous damping coefficients C_e and total Coulomb friction forces F_{μ_e} obtained by the two methods differ by about 3%. The results obtained by the least-squares approach lead to slightly larger dissipative forces (3%), but the differences, amounting to about 2 kN for a velocity of 1 m/s, are well below the margin of error in estimating the dissipative forces from the measured data.

The main finding of the paper is that the least-squares approach appears to be equally capable of identifying the key system parameters from scaled earthquake tests, and periodic sinusoidal and triangular tests. For white noise tests, the least-squares approach leads to the correct effective mass, and the correct total friction force if the viscous damping coefficient is constrained, but the values obtained for the effective stiffness are in error. The smaller the amplitude of the white noise tests, the larger the error in the estimate of the effective stiffness. If the viscous damping coefficient is left unconstrained, the identified values for the friction force and viscous damping coefficient from white noise tests are very different from those estimated from periodic and earthquake tests.

The NEES-UCSD shake table mechanical subsystem considered, which does not include the effects of the oil columns in the actuators, has a frequency of 0.47 Hz that is clearly observable in the theoretical and experimental steady-state frequency response curves for the system. This characteristic frequency is, of course, very different from the oil column frequency, which for the NEES-UCSD shake table system is 10.66 Hz. The theoretical dynamic amplification (or frequency response) curves depend on the amplitude of the actuator force and match closely the experimental results.

As part of the study presented herein, it has also been found that the relationship between the viscous forces and table velocity is not linear, but can be represented by a power law, that the friction forces on the vertical bearings can be separated from those on the lateral bearings, and that the dissipative forces typically represent a very small fraction of the total actuator force.

Acknowledgments

This work was supported by the National Science Foundation through the NEES program, Grant No. CMS-0217293; the Englekirk Center Board of Directors and NEESinc through a NEES facility enhancement project, and Lawrence National Laboratory (with Dr. Dave McCallen as research manager). These sources of support are gratefully acknowledged. The writers want to thank Prof. José Restrepo (U.C. San Diego), Prof. Tomaso Trombetti (University of Bologna, Italy) for their significant contributions during the shake-down and characterization tests that produced the data used in this study. Any opinions, findings, and conclusions or recommendations expressed in this paper are those of the writers, and do not necessarily reflect those of the sponsors.

References

- Clark, A. (1992). "Dynamic characteristics of large multiple degrees of freedom shaking tables." *Proc., 10th World Conf. on Earthquake Engineering*.
- Conte, J. P., and Trombetti, T. L. (2000). "Linear dynamic modeling of a uniaxial servo-hydraulic shaking table system." *Earthquake Eng. Struct. Dyn.*, 29(9), 1375–1404.
- Crewe, A. J., and Severn, R. T. (2001). "The European collaborative programme on evaluating the performance of shaking tables." *Philos. Trans. R. Soc. London, Ser. A*, 359, 1671–1696.
- Hwang, J. S., Chang, K. C., and Lee, G. C. (1987). "The system characteristics and performance of a shaking table." *NCEER Rep. No. 87-0004*, National Center for Earthquake Engineering Research, State Univ. of New York at Buffalo, Buffalo, N.Y.
- Kusner, D. A., Rood, J. D., and Burton, G. W. (1992). "Signal reproduction fidelity of servohydraulic testing equipment." *Proc., 10th World*

- Conf. on Earthquake Engineering*, Rotterdam, The Netherlands, 2683–2688.
- Ozcelik, O., Luco, E. J., Conte, J. P., Trombetti, T. L., and Restrepo, J. I. (2007). “Experimental characterization, modeling and identification of the UCSD-NEES shake table mechanical system.” *Earthquake Eng. Struct. Dyn.*, in press.
- Rinawi, A. M., and Clough, R. W. (1991). “Shaking table-structure interaction.” *EERC Rep. No. 91/13*, Earthquake Engineering Research Center, Univ. of California at Berkeley, Berkeley, Calif.
- Shortreed, J. S., Seible, F., Filiatrault, A., and Benzoni, G. (2001). “Characterization and testing of the Caltrans seismic response modification device test system.” *Philos. Trans. R. Soc. London, Ser. A*, 359, 1829–1850.
- Thoen, B. K. (2004). *469D seismic digital control software*, MTS Corporation.
- Thoen, B. K., and Laplace, P. N. (2004). “Offline tuning of shaking table.” *Proc., 13th World Conf. on Earthquake Engineering*, Vancouver, B. C., Canada, Aug. 1–6, Paper No. 960.
- Trombetti, T. L., and Conte, J. P. (2002). “Shaking table dynamics: Results from a test analysis and comparison study.” *J. Earthquake Eng.*, 6(4), 513–551.
- Twitchell, B. S., and Symans, M. D. (2003). “Analytical modeling, system identification, and tracking performance of uniaxial seismic simulators.” *J. Eng. Mech.*, 129(12), 1485–1488.
- Van Den Einde, L., et al. (2004). “Development of the George E. Brown Jr. network for earthquake engineering simulation (NEES) large high performance outdoor shake table at the Univ. of California, San Diego.” *Proc., 13th World Conf. on Earthquake Engineering*, Vancouver, B.C., Canada, August 1–6, Paper No. 3,281.
- Williams, D. M., Williams, M. S., and Blakeborough, A. (2001). “Numerical modeling of a servohydraulic testing system for structures.” *J. Eng. Mech.*, 127(8), 816–827.